Design and Test of Reverse Osmosis Pressure Cell for *in-situ* Small-Angle Neutron Scattering Studies

Dietmar Schwahn[a,*] , Herbert Feilbach[b], Thomas Starc[b], Vitaliy Pipich[c], Roni Kasher[d], Yoram Oren[d,*]

[a] Technische Universität München, Forschungs-Neutronenquelle Heinz Maier-Leibnitz (FRM II), D-85748 Garching, Germany.

[b] Forschungszentrum Jülich GmbH, Jülich Centre for Neutron Science JCNS and Institute for Complex Systems ICS, D52425 Jülich, Germany.

[c] Jülich Centre for Neutron Science JCNS-FRM II; Outstation at FRM II, D-85747 Garching, Germany.

[d] Zuckerberg Institute for Water Research, Jacob Blaustein Institutes for Desert Research, Ben-Gurion University of the Negev, Sede Boqer Campus 84990, Israel.

* Corresponding authors. Tel.: +49 (0)2461 616661; fax: +49 (0)2461 612610.

E-Mail address: d.schwahn@fz-juelich.de (D. Schwahn).

Tel.: +972-8-6563530

E-mail address: yoramo@bgu.ac.il (Y. Oren)

ABSTRACT

We introduce a new method for real-time studying of membrane scaling and biofouling on thin film membranes in reverse osmosis, nanofiltration water treatment processes using *in-situ* small-angle neutron scattering (SANS). SANS delivers information on nano and microscopic structures that support the interpretation of relevant engineering parameters such as membrane permeability and water flux. A high pressure SANS flow cell is described, followed by SANS characterization of thin-film composite reverse osmosis membranes finding ~0.5 μm large cavities and ~300 Å diameter large rod-like cavities inside the non-woven polyester and micro-porous polysulfone layer, respectively. This is followed by presentation of *in-situ* desalination experiments in cross-flow mode at applied pressures of 6 bars and feed flow velocity of 0.2 cm/s. The scattering cross-section (Σ_t) derived from the transmission coefficient of non-scattered neutrons became a relevant parameter as it is a measure of the total scattered neutrons. The overall enhancement of Σ_t is accompanied by reduced membrane permeability measured in parallel. After finishing the process of desalination the membranes showed enhanced scattering from μm large domains of mass fractal structure.

Keywords: Small-Angle Neutron Scattering; *In-situ* reverse osmosis wastewater desalination; RO membrane; Scaling, Organic fouling; Bovine serum albumin, BSA.

Abbreviations

- SANS — small-angle neutron scattering
- T — transmission coefficient of neutrons
- μ_t — sum of linear coefficients of neutron absorption, incoherent and SANS scattering
- A — scattering amplitude
- $d\Sigma/d\Omega$ — differential macroscopic cross-section
- Σ_t — total macroscopic cross-section
- Σ_{abs} — total absorbing macroscopic cross-section
- Σ_{SANS} — total macroscopic cross-section of SANS
- Q2 — second moment with meaning of the invariant of scattering
- b — coherent scattering length
- ρ — coherent scattering length density
- $\Delta\rho^2$ — scattering contrast
- Ω_M — volume of molecule
- δ — scattering angle
- λ — wavelength of neutron
- $\underline{Q}$ — momentum transfer
- $\underline{k}$ — wavenumber
- $R_{g.}$ — radius of gyration
- P_4 — Porod constant
- α — exponent of power law of $d\Sigma/d\Omega$ at $Q > 1/R_g$
- V_p, S_p, N_p, Φ_p — volume, surface, number density, and volume fraction of domains exposed to scattering.
- l_C — coherence length of domains
- D_S — thickness of sample
- HAP — hydroxyapatide
- PMP — protein mineral particle

- RO reverse osmosis
- NF nanofiltration
- TFC thin-film composite
- TMP trans membrane pressure
- SSE simulated secondary effluent

1. Introduction

The strong demand for potable water in arid areas around the globe is leading to an increasing number of sea, brackish and wastewater desalination plants using reverse osmosis (RO) and nanofiltration (NF) technologies. Despite this vast activity, fresh water supply in many countries, especially those that are remote from the sea, is still a serious problem. In these cases, recycling of impaired water such as municipal wastewater, to a level of unlimited application is a reasonable solution. In fact, this is done today in several locations around the globe such as in Singapore, Windhoek (Namibia), Orange County (CA, US) and Kuwait and is considered by many other countries. Another, not less important aspect of recycling is protection of the environment. Membrane-based technologies are extensively used today in these respects.

A serious problem in RO/NF desalination of municipal wastewater is biofouling and scaling of the membranes, limiting membrane efficiency and lifetime [1,2,3]. Ning et al. [4] reported that calcium phosphate and organic matter accumulated on the RO-membrane, suggesting that nanoparticles pass through microfiltration and ultrafiltration membranes, ending up on RO-membranes as a cake-layer fouling. In particular scaling by calcium phosphate in municipal wastewater treatment systems is a severe problem as no efficient antiscaling agents are currently available [5].

Calcium-phosphate mineral formation during RO wastewater desalination was studied using surface pressure−area isotherms and spectroscopic analyses of a solution simulating the ionic profile of domestic secondary-treated wastewater effluents (termed simulated secondary effluent - SSE); it was found that calcium phosphate mineralization was accelerated by organic chemical groups that are present on biofouled membranes [6]. In this respect the issue of biofouling-induced scaling is, to a large extent, strongly linked to bio-mineralization [7]. In addition, recent small-angle neutron scattering (SANS) experiments by the authors showed strong influence of organic molecules present in biofilms on mineralization in a model synthetic salt solution [8,9]. Proteins such as BSA, lysozyme and the polysaccharide alginate (AA) added to the solution, induced within a few seconds strong precipitation of nearly μm large composite particles composed of organic components as well as calcium phosphate and carbonate. In another study gold-nanoparticles were used as templates for studying surface mineralization by SANS in model solutions for wastewater desalination [9,10]; for example it was found that BSA-gold

nanoparticles induced fast precipitates of 0.2 μm that were composed of 50% - 80% minerals, identified as calcium phosphate and calcium carbonate.

In this manuscript we report on developing of a new cell for *in-situ* SANS studies of fouling and scaling of thin film composite (TFC) RO/NF membranes. Application of SANS to polymeric TFC membranes appears rational, as static and kinetic properties of polymers are studied with neutron scattering methods [11,12]. Similar *in-situ* SANS experiments on ceramic ultrafiltration membranes are reported in [13]. Filtration of aqueous BSA solutions of different pH values was explored and compared with the permeate flux. Another *in-situ* SANS measurements studied the formation of a cake layer at the surface of an ultrafiltration membrane which was exposed to a 0.48% aqueous Laponite solution at a transmembrane pressure of 0.5 bar [14].

Currently, several non-invasive real-time methods are presented in literature and demonstrated their application in membrane processes. Greenberg and coworkers developed the ultrasonic time-domain reflectometry (UTDR), where the membrane surface is monitored by sensing the reflection of ultrasonic radiation from the membrane [15]. The UTDR was proved efficient in studying membrane characteristics, as well as monitoring membrane fouling and biofouling [16,17]. However the detection of biofilm and scaling on membrane surfaces is still a significant challenge for UTDR due to the small difference in acoustic properties at the fouling/membrane and fouling/feed solution interfaces [16]. Electrical impedance spectroscopy (EIS) was also demonstrated as a membrane monitoring and characterization technique, as was applied for studying membrane fouling [18,19,20,21,22]. Nevertheless, unlike UTDR or SANS it is in essence an invasive technique that requires special arrangements to provide the proper electrical connections. SANS might be outstanding with respect to other tools as the just mentioned ones that it is enabling basic studies of membrane phenomena and distinguishing between inorganic and organic fouling via contrast variation and their evolution during desalination on a level of microscopic length scale under most realistic real-time conditions. It is the main goal of this effort to elucidating the influence of biofluing on scaling using *in-situ* SANS monitoring at conditions that are close to those prevailing in actual membrane processes.

2. Theoretical Background of SANS.

Scattering of photons and, as in our case, neutrons occurs in momentum (P-) space in contrast to optical, electron (TEM) and atomic force (AFM) microscopies which are reproducing their results in real (R-) space. This implies that scattering methods do not provide pictures of our real world but rather of the so-called reciprocal or the momentum space [23]. The coordinates of the reciprocal space are formed by the components of the scattering vector Q which corresponds to the momentum transfer ΔP (the symbols Q and ΔP are representing vectors) of the neutrons and are interrelated via the well-known de Broglie relationship $\Delta P = hQ$ (h, Planck constant h divided by 2π). The absolute value of the scattering vector Q is determined from the scattering angle δ and wavelength λ of the neutrons (in the present case, λ = 12.8 Å), according to $Q = 4\pi/\lambda \sin(\delta/2)$. It is a rule of thumb that scattering from objects of radius R mainly occurs in a Q regime of the order of 1/R, i.e. Q ~ 1/R.

The scattering techniques of neutrons and photons are well established tools both from theoretical and experimental aspects. Scattering occur at domains which differ from their

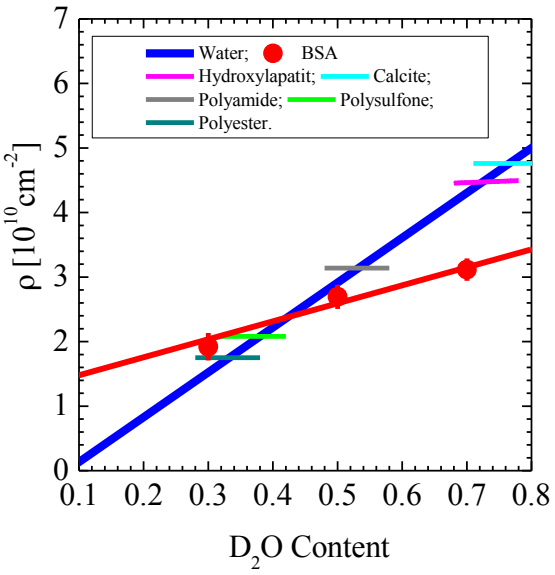

Figure 1. Coherent scattering length densities ρ of water and protein BSA in aqueous solution as a function of D_2O volume fraction ρ of the crystalline minerals hydroxyapatite (HAP) and calcite as well as the polymers of the RO-membrane are indicated as short lines when crossing ρ (blue line) of the H_2O/D_2O mixture.

surroundings with respect to chemical composition and/or mass density. Examples of those domains are precipitates and cavities in solid matrices or colloids in solution. The differences in chemical composition and/or mass density are expressed by the scattering contrast. For neutrons the scattering contrast is determined by the square of the difference of the coherent scattering length density of the domain (P) and its surrounding (S), namely $\Delta\rho^2 = (\rho_P - \rho_S)^2$. The scattering length density is defined as the sum of the coherent scattering length of the atoms, b_i, of a molecule divided by its volume Ω_M, that is $\rho = \sum_i b_i / \Omega_M$ [23,24]. Figure 1 shows the coherent scattering length density ρ of molecules of the present study as a function of D_2O content of an aqueous solution. As seen in the figure the parameter ρ of H_2O and D_2O shows very different values and allows a continuous change of ρ by mixing H_2O with D_2O. The reason for that is that neutrons interact with the nucleus of atoms and therefore deliver individual values of coherent scattering length for isotopes as tabulated in [24]. The very different scattering of neutrons at hydrogen (b_H = - 0.3739×10^{-12}cm) and deuterium (b_D = 6.671×10^{-12}cm) is extensively used as a tool to enhance scattering contrast or to match scattering for identifying particular domains, as also done in the present study.

The scattering length density ρ of BSA was determined experimentally in [8], whereas ρ of the stable polymorphs of calcium phosphate and carbonate was evaluated as compiled in Table A1. The observed change of ρ for proteins with the amount of D_2O is due to H/D exchange at their outer surface [25]. The scattering contrast $\Delta\rho^2$ of the proteins becomes zero in water of about 42% D_2O content, implying that the protein becomes invisible for neutrons at this D_2O content. On the other hand, minerals such as hydroxyapatite (HAP) and calcite become invisible in water of about 75% D_2O content as visualized in Figure 1 by the equality of the corresponding ρ's. The large difference of scattering contrast of proteins and minerals and the possibility of their matching in H_2O/D_2O mixtures offers the opportunity of identifying organic and inorganic phases of stable micron-scale protein-mineral particles (PMPs) as observed in a recent study by SANS [8].

The fact that neutrons are electrically neutral implies that they are penetrable through most materials for several tenths of cm without significant attenuation. Taking advantage of this property allowed us to build a RO-cell for *in-situ* studies of reverse osmosis (RO) desalination as

will be described in detail below. Small-angle neutron scattering is a quantitative method determining structural parameters averaged over macroscopic large volumes of the order of 0.1 cm^3. In this respect it is complementary to TEM in which individual domains are made visible. The scattered neutron intensity is measured as a function of the momentum transfer Q and determined as differential macroscopic cross-section $d\Sigma/d\Omega$ in units of cm^{-1} (i.e. scattering per cm^3 of sample volume). It is referred here to scattering that emerges from individual domains that neglect possible coherence effects from ordering of the domains by long range interaction or excluded volume interaction. For the analyses of scattering pattern we used the Beaucage Equation [26]:

$$\frac{d\Sigma}{d\Omega}(Q)=\frac{d\Sigma}{d\Omega}(0)\exp(-u^2/3)+P_\alpha\left[\left(\mathrm{erf}\left(u/\sqrt{6}\right)\right)^3/Q\right]^\alpha \qquad (1)$$

In this expression, u is the product of Q and radius of gyration R_g.. At $Q < 1/R_g$, $d\Sigma/d\Omega$ is determined by the first term and corresponds to Guinier's approximation whereas at $Q > 1/R_g$ scattering often follows a power law with the exponent α. In many cases $\alpha=4$ (Porod's law) is valid indicating 3-dimensional domains with smooth interface. The parameters $d\Sigma/d\Omega(0)$ and P_4 of Eq. (1) are expressed as

$$\frac{d\Sigma}{d\Omega}(Q=0)=\Phi_P\left(1-\Phi_P\right)V_P\left[\rho_P-\rho_S\right]^2 \text{ and } \qquad P_4=2\pi N_P S_P\left[\rho_P-\rho_S\right]^2, \qquad (2)$$

and determine volume V_P, surface S_P, volume fraction Φ_P, as well as number density N_P of the scattering generating domains [23]. An important parameter is determined from the integral $\frac{1}{4\pi}\int d\Sigma/d\Omega(\underline{Q})\, d_3\underline{Q}$ over the reciprocal space representing the "invariant" Q2. This parameter is termed "invariant" as it is independent of domain size and only proportional to the domain volume fraction and their scattering contrast as expressed in Eq. (3) [23].

$$Q2=2\pi^2\ \Phi_P\left(1-\Phi_P\right)\Delta\rho^2 \qquad (3)$$

A particular scattering law will be needed for analyzing the porous support layer of thin film composite (TFC) membranes made of about 40 μm thick polysulfone transporting the effluent via small channels of the order of 150 Å average diameters as will be described in more detail below

in section 4.1. Since the momentum transfer Q is oriented perpendicular to the axis of the channels we find for the form factor of rods the expression

$$\frac{d\Sigma}{d\Omega}(Q) = \frac{d\Sigma}{d\Omega}(0)\left[2J_1(u)/u\right]^2 \qquad (4)$$

with u=RQ (R radius of a rod) and J_1 a Bessel function of the first order [27].

Another relevant SANS parameter is the transmission of the primary neutron beam, i.e. neutrons which are not scattered but rather go through the sample. Transmission expresses the intensity drop of the incoming neutron beam caused by scattering and absorption by the sample. The incoming neutron beam is monochromatic (usually with half width of $\Delta\lambda/\lambda$=0.10, λ is wavelength of neutrons) of selected divergence due to velocity selector and collimator. A collimator is usually realized by two apertures made from neutron absorbing materials [28]. In special cases such as for very-small-angle scattering (VSANS), optical devices such as refractive lenses [29] or ellipsoidal mirror [30] focus the neutron beam on the detector. Such a mirror is implemented in the instrument KWS3 for the use in the present experiments.

The transmission T represents an integral number of scattered neutrons over the whole space angle Ω of the Ewald sphere and is expressed by the total scattering cross-section $\Sigma_t = \int d\Sigma/d\Omega\, d\Omega$ times the thickness D_S of the sample in Eq. (5). A decrease or increase in

$$T = \exp\{-\mu_t\} = \exp\{-\Sigma_t D_s\} \qquad (5)$$

transmission denotes an increase or decrease of scattering intensity, respectively. The parameter $\mu_t = \Sigma_t D_s$ represents the sum of linear coefficients of neutron absorption, incoherent and small-angle scattering as discussed in [31]. In the RO-cell there is strong contribution of SANS scattering from the membrane as will be shown later and only a small contribution is expected from precipitation and fouling at the membrane surface. Therefore, it is important to consider the transmission in conjunction with the scattered beam. As already mentioned in context with Eq. (5) the transmission is mainly determined by the total scattering Σ_t. The cross-section from small-

$$\Sigma_{SANS} = \int_{4\pi} \frac{d\Sigma}{d\Omega}\left(\underline{Q}\right) d\Omega = \frac{1}{k^2}\int_{4\pi} \frac{d\Sigma}{d\Omega}\left(Q\right) d_2Q \qquad (6)$$

angle scattering, Σ_{SANS}, is determined from the integral over the total space angle $d\Omega = d_2Q/k^2$ with the wavenumber $k=2\pi/\lambda$ (λ neutron wavelength) (Eq. (6)). In case of isotropic scattering Q becomes a scalar and one gets

$$\Sigma_{SANS} = \frac{2\pi}{k^2}\int_0^\infty Q\frac{d\Sigma}{d\Omega}(Q)\, dQ. \qquad (7)$$

Accordingly, one can evaluate the transmission coefficient from the experimental $d\Sigma/d\Omega(Q)$ for comparison with the experimental transmission coefficient (Eqs. (7) and (5)).

In summary, structural information of colloids in the feed as well as of precipitates and cavities inside the membrane is provided from fitting the scattering laws (Eqs. (1) and (4)) to the experimental macroscopic scattering cross-section $d\Sigma/d\Omega(Q)$. The knowledge of scattering contrast $\Delta\rho^2$ obtained from contrast variation allows identification the domains, whereas the so-called invariant Q2 in Eq. (3) delivers the domain volume fraction Φ_p. Another important parameter is the neutron transmission coefficient T which is helpful in determining the total scattered cross-section Σ_t.

3. Experimental

Real-time SANS desalination experiments were performed with a flat-sheet XLE-440 RO membrane from Dow Filmtech (Minneapolis, MN, USA). Water permeability was determined with deionized water and with SSE solution mentioned above. SSE is a model solution for the mineral components of secondary-treated domestic wastewater in desalination with 80 - 85% recovery of a Shafdan (Israel) municipal wastewater treatment plant prospective desalination plant. Its composition is given in details in [6]. Scattering was taken from membranes while in air and also in salt-free water with varying degree of D_2O content in order to determine size and scattering contrast of the scattering centers as explained above.

Despite its small thickness (140 μm), the above TFC membrane surprisingly showed strong scattering for neutrons which to large extent is created by cavities inside the polyester non-woven supporting material as its scattering length density ρ is large (see Table A1). This is a serious disadvantage that can be greatly overcome by equilibrating the membrane with a H_2O/D_2O salt solution using a ratio matching the scattering length density of the membrane polymers. In

practice, the scattering from any pristine membrane is determined before exposing the membrane to salt solutions as a reference for the treated membrane.

3.1. Design of a Pressure Cell for in situ SANS Studies of Membrane Processes

We constructed a cell for *in-situ* explorations of TFC membrane structural properties as well as membrane fouling during reverse osmosis (RO) desalination using SANS. Such a cell has to fulfill several conditions: (i) It should allow running the RO process either as cross-flow or dead-end mode (preferably cross-flow) under suitable pressures and the use of different types of membranes. (ii) It should be guaranteed that the strength of neutron scattering from the fouling materials at the membrane's surface is sufficiently strong in comparison with scattering from the other components in the neutron beam track. This demand was difficult to achieve as neutrons also have to penetrate through the membrane and supporting spacer as well as the cell's structural material. The schematic diagram of the RO flow-cell in Figure 2 shows a cross-sectional view in

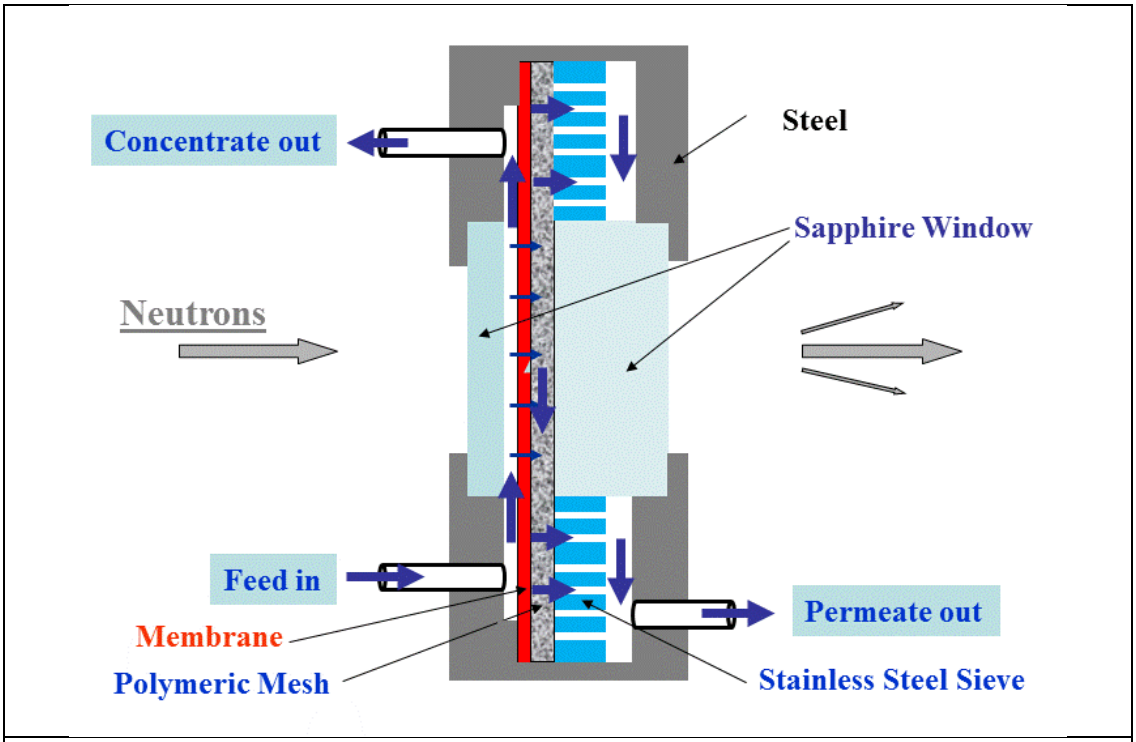

Figure 2. Schematic design of the RO flow-cell for *in-situ* small-angle neutron scattering (SANS). Distance between the sapphire windows 0.15 cm.

the direction of the neutron beam. The neutrons enter and leave the cell via sapphire windows of 3 cm in diameter, which are transparent to neutrons with negligible diffraction and allowing feed pressure up to 6 bar. There are three circular windows on each side for neutron passage in order to allow studies at different positions along the membrane. The window's diameter was set according to the beam area at the instrument KWS3 for very-small angle neutron scattering (VSANS).

Figure 3 gives a close-up look at the RO cell and a photograph of the experimental setup. The thicknesses of the sapphire windows at the two sides are not equal in order to properly support the membrane against the stainless steel sieve as seen in Figure 2, thus keeping it flat. In the present experiments we exposed only the central window out of the three and membrane to neutrons.

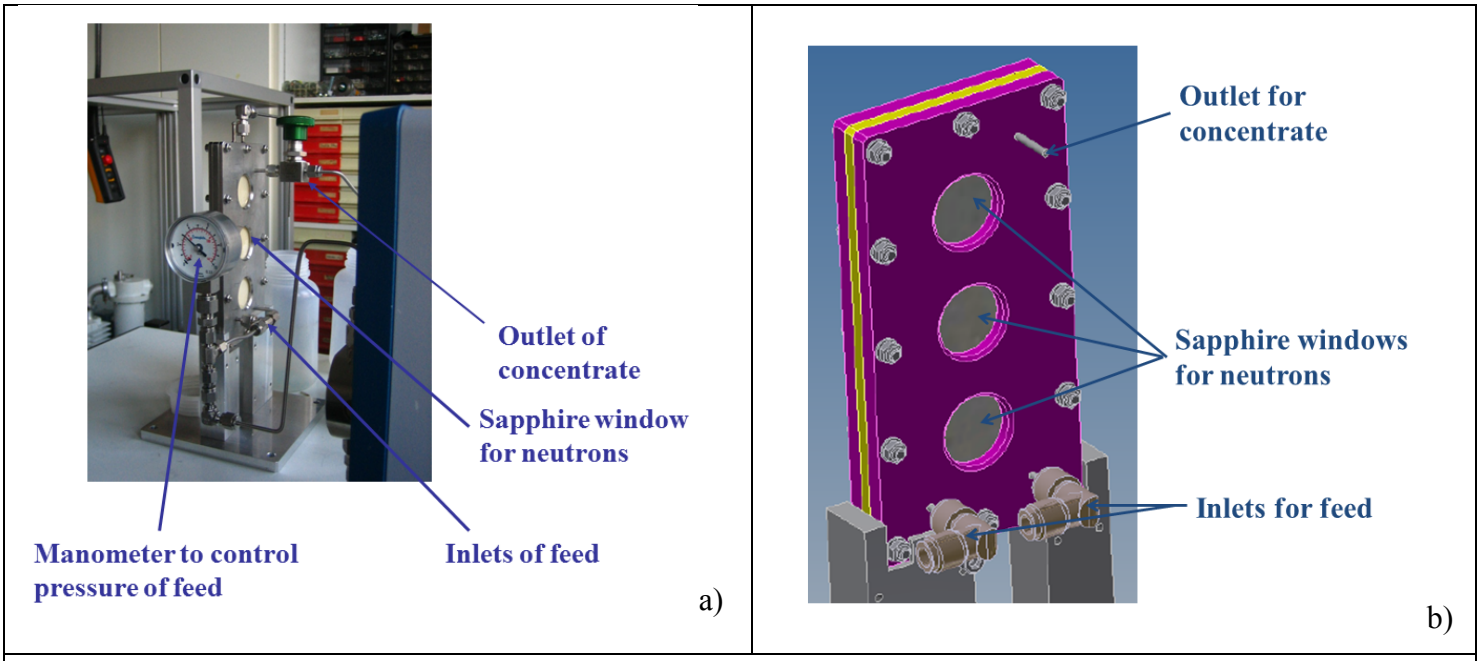

Figure 3. a) A photograph of the SANS RO-cell. b) RO-cell setup. The three sapphire windows mark possible positions for the neutron beam to pass the cell.

The membrane dimensions exposed to the flowing solution are 11 by 4.5 cm and the feed channel height is 0.14 cm. This channel is packed with a standard polyester mesh spacer taken from a RO module. There are two tubes at the bottom of the cell as inlet for the SSE as the feed. The two inlet tubes are necessary for a more homogeneous flow distribution over the width of the

membrane in the cell. DI water or SSE solution were applied to the feed channel at a linear flow rate of 0.2 cm sec^{-1} by a centrifugal pump. At the top of the cell there is another tube for the concentrate outlet. A pressure adjusting valve is connected to this tube, which can be closed thereby allowing switching between dead-end and cross-flow modes. The permeate outlet is located at the bottom of the cell in order to avoid a water layer on the pathway of the neutrons at the permeate side.

3.2 Neutron Background Scattering of the RO-Cell

In this section we present scattering patterns from a dry cell with and without a spacer and a membrane as depicted in Figure 4. The measurements were performed in the low Q range of the VSANS instrument KWS 3. The scattering pattern from the empty cell is rather flat in the range of 10 to 10^3 cm^{-1} as expected from scattering of the two sapphire windows along the beam

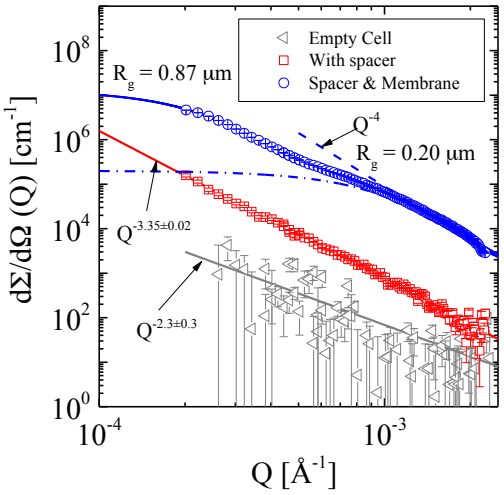

Figure 4. Scattering pattern in low Q range for the empty RO-cell, with a polyester spacer and spacer plus RO membrane. Strong contribution of the membrane showing scattering centers of different size (indicated by the two R_g's) is demonstrated. The statistical error bar of the spacer and membrane scattering are smaller than the symbol size.

pathway. The cell with a polyester spacer shows a stronger scattering, following a power law with an exponent slightly larger than 3, whereas the membrane generate a further two orders of magnitude increase of scattering. The scattering from the membranes show a bimodal size

distribution with radii of gyration of 0.87 μm and 0.20 μm and a Q^{-4} power law at large Q according to the Porod law (Eq. (2)) [23]. The amplitude of Porod's law (P_4) is a measure of the total surface area of the scattering domains ($N_4 \times S_P$) per unit cm^3 of sample volume (Eq. (2)). As a result, we find strong undesired scattering from the spacer and the membrane, which is expected to overlap with scattering from any organic and inorganic fouling components formed during the filtration process. Scattering from protein-mineral particles at Q = 0 induced by BSA in SSE solution in our former work was of the order of 3×10^3 cm^{-1} [8]. This implies that the measuring signal is in the range of parts per thousand with respect to background scattering from spacer and membrane. This suggests that for these experiments, membranes that are made of a nonwoven support of less scattering than polyester (e.g. polypropylene) are preferable.

4. Results and Discussion

4.1.Out-of-Cell SANS Measurements with RO TFC Membranes

In this section we present SANS experiments on TFC RO-membrane samples that were exposed to air and to salt-free water. These measurements are required as reference for studies of membrane fouling in the high pressure cell.

4.1.1. TFC RO-Membrane in Air

Typically, TFC RO-membranes are composed of an aromatic polyamide film of 100 to 250 nm thickness on top of a ~ 40 μm thick micro porous polysulfone layer. These two layers are supported by a third layer – either polypropylene or polyester – consisting of a ~100 μm thick non-woven fabric. The aromatic polyamide skin layer is highly cross-linked whereas the fraction of the cross-linked polyamide repeating units from total polyamide units is about 65% [32,33, 34]. Figure 5 shows a schematic drawing of such a composite membrane which in our case had athickness of 140 μm. The neutron flux is directed perpendicular to the membrane surface implying that the momentum transfer Q is oriented in parallel to the membrane surface as shown by the red arrow in Figure 5. This implies that structures only in direction to Q, namely, perpendicularly to the flow direction of the neutrons, give rise to scattering. This is understood

from the phase factor of the scattering amplitude which is a complex number according to $A(\underline{Q}) = \int_{V_S} d_3\underline{r}\,\rho(\underline{r})e^{i\underline{Q}\,\underline{r}}$ (V_S volume of sample and $d\Sigma/d\Omega(\underline{Q}) \propto |A(\underline{Q})|^2$); the scalar product of $\underline{Q}$ and $\underline{r}$ shows that diffraction is determined by the structure in direction of $\underline{Q}$ [24]. A scattering pattern of such a membrane in air is shown in Figure 6 (a). The data show the typical shape from scattering centers of two different sizes. The data therefore were fitted with two superposed Beaucage expressions (Eq. (1)) whose results are shown by the red solid line describing the data at Q smaller than 10^{-2} Å^{-1}. It has to be mentioned that the data were obtained at two SANS

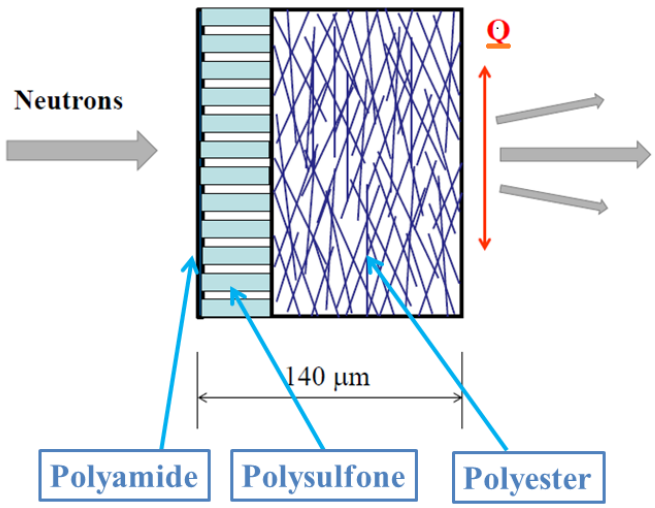

Figure 5. Schematic design of a thin film composite RO membrane as related to neutron scattering. The three layers are of aromatic polyamide (100-200 nm thick), porous polysulfone (about 40 µm thick), and polyester (about 100 µm thick). The overall thickness of the present membrane is ~140 µm.

instruments, namely the KWS 3 and the pinhole KWS 2 covering a Q range of three orders of magnitude from 10^{-4} to 10^{-1} Å^{-1}. These data were corrected with respect to background scattering and normalized in absolute units by a secondary standard and the thickness of the membrane sheet of 140 µm. Two radii of gyration (R_g) could be determined, namely, 0.86 and 0.22 µm, which, if representing scattering centers of spherically shaped entities such as cavities would correspond to mean diameters of 2.2 and 0.57 µm, respectively. At larger Q the intensity follows

the Q^{-4} Porod law characteristic for three dimensional domains with sharp interfaces whose amplitude P_4 determines the total domain surface area per cm^3 (Eq. (2)). At Q larger than 10^{-2} $Å^{-1}$ we observe weak deviation from the Q^{-4} power law. This deviation of scattering is depicted in Figure 6b showing an oscillatory shape. The origin of this scattering is interpreted as coming from the porous structure of the polysulfone layer. This scattering was fitted with the form factor of the cylinder in Eq. (4) giving a diameter of nearly 300 Å which is about a factor of 2 smaller than given for the average pore diameter (700 Å) in the polysulfone layer of a TFC membrane studied by Singh et al. [34]. For simplicity we assumed mono-dispersed single rods. Polydispersity of the rods in combination with instrumental resolution smear out the oscillatory behavior of the form factor at larger Q in consistence with the scattering data.

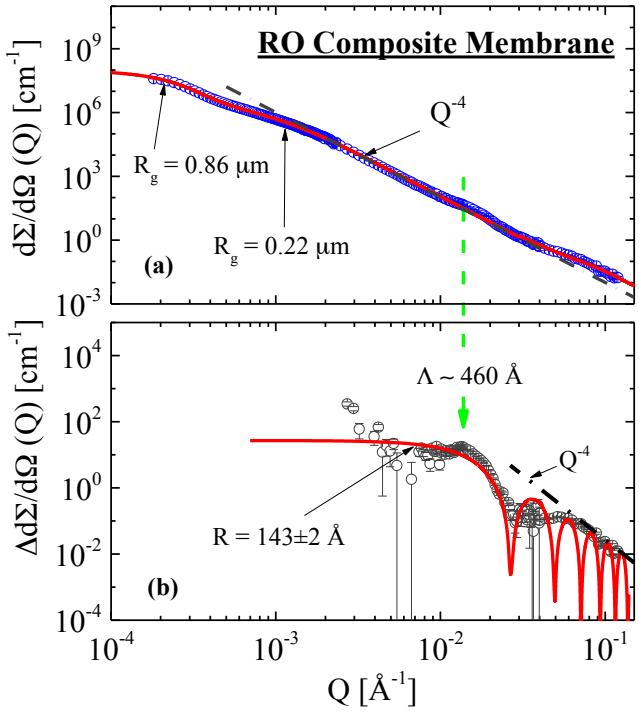

Figure 6. a) Thin film composite membrane in air; b) Porod scattering (Eqs. (1) and (2); $P_4 \times Q^{-4}$) subtracted from membrane scattering whose difference is interpreted as caused by the porous structure of the polysulfone layer.

The corresponding scattering length densities ρ of polysulfone and polyester are given in Table A1; in an aqueous solution of nearly 40% volume (39.91% mole fraction) content of D_2O the scattering of cavities in the two support layers would be near zero, i.e. become matched with the solvent. The thinner polysulfone layer is made compact with rod like channels of small diameter (~300 Å) in order to resist the external pressure field. It seems therefore reasonable to conclude that the main component of scattering has its origin from the large fraction of cavities in the non-woven part of the support material. This conjecture gets support from the data in Figure 6 and the second moment Q2 (Eq. (3)) of the rod scattering, which has a value of about 6.1×10^{-5} cm^{-1} $Å^{-3}$ and corresponds to a volume fraction of 0.7%. More information on this issue is obtained from contrast variation experiments presented in the next section.

4.1.2. Composite RO-Membranes in Salt-free Water – Equilibration and Matching

In a next step scattering of neutrons from TFC membranes after equilibration with salt-free mixtures of H_2O/D_2O in standard quartz cuvettes was determined. This experiment is important because it determines the mean scattering length density, i.e. the average scattering contrast of the

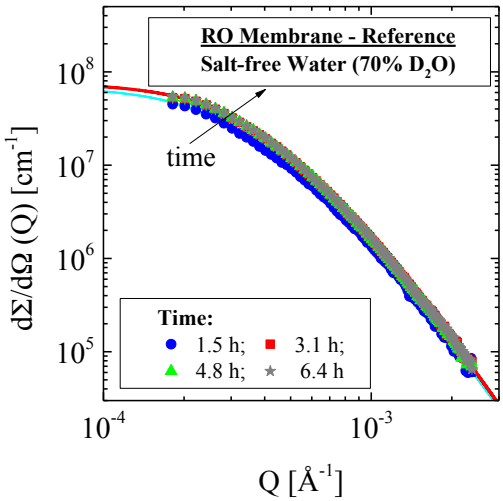

Figure 7. Scattering patterns of RO-membranes in salt-free water (70% D_2O) at various time intervals. After about 3 hours the membrane showed constant scattering.

membrane scattering domains in water and determines the mixture of H_2O/D_2O with the lowest scattering from the membrane for an optimized condition of the desalination experiments under the prescribed conditions. Figure 7 depicts a selection of scattering data from a reference membrane as a function of equilibration time in salt-free water with 70% D_2O. These experiments were performed at the VSANS instrument KWS 3 in order to determine the size of the larger scattering centers as well. A small increase of scattering is observed during the first hours of exposure before becoming stable after about 3 hours. Constant scattering indicates reaching equilibration, i.e. completion of filling the pores of the polysulfone and non-woven support of the membrane with water.

Scattering of the membrane shows strong change when exposed to water of varying D_2O content. The reason is the large difference of coherent scattering length density ρ_W of H_2O and D_2O as shown in Figure1. The membrane was tested in water of varying H_2O/D_2O content as depicted in Figure 8a, showing the scattering patterns in H_2O as well as in mixtures of different

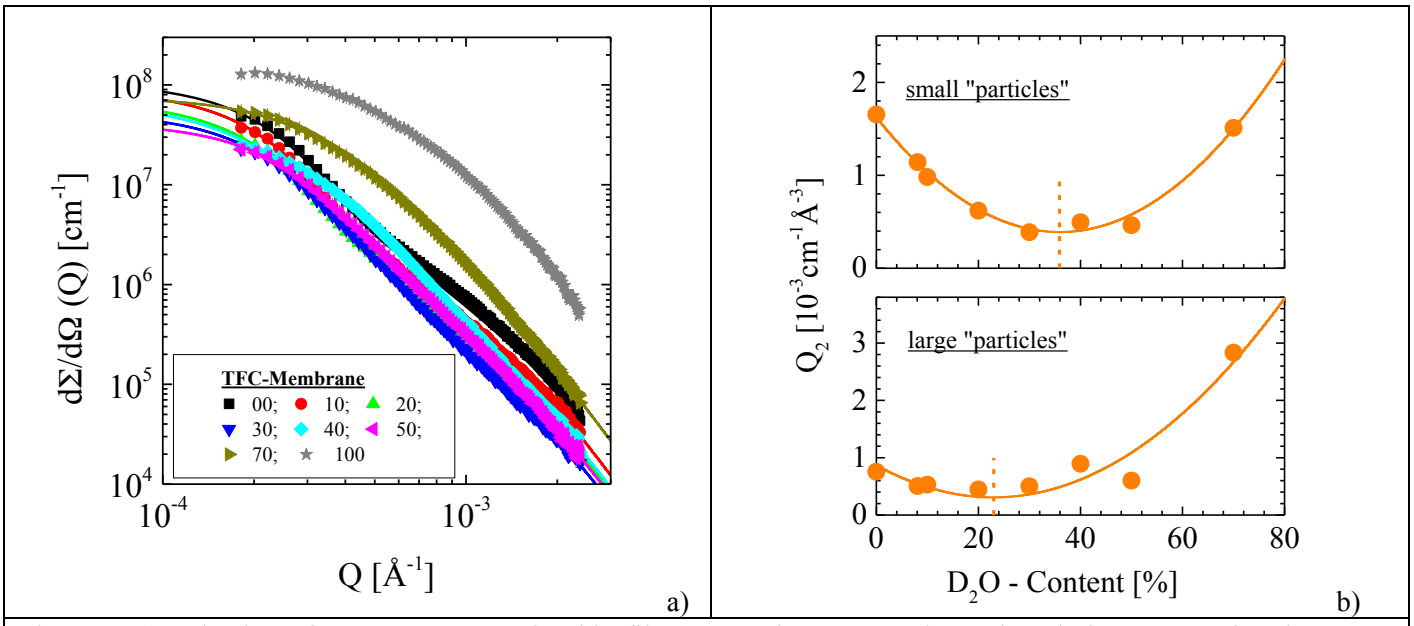

Figure 8. a) Selection of SANS patterns of a thin film composite RO-membrane in salt-free water of various D_2O fractions (given in [%] as noted by the colored symbols). b) Second moment Q2 of small and large scattering centers of the membranes versus D_2O content.

D_2O content in the range 0 to 100%. The solid lines represent a fit of the data with Eq. (1). The second moments Q2 of the large and small scattering centers were determined from the fitted

scattering curves and plotted versus D_2O content in Figure 8b (the corresponding numerical values are compiled in Table A2 in Appendix A). Q2 is a robust parameter as it represents an integral number of the scattering curve and it only depends on volume fraction and scattering contrast of the scattering domains according to Eq. (3), with $\Delta\rho = \left[\rho_P - \rho_W\right]$ (coherent scattering length densities are plotted in Figure 1 and compiled in Table A1). We could not use the scattering data of the 100% D_2O solution for analysis as scattering became too strong, implying that the scattering contrast is too large and dominating by multiple scattering. The Q2 values in

$$Q2 = A \times \left(\varphi_{D_2O} - \bar{\varphi}_{min}\right)^2 + Q2_{const.} \quad (8)$$

Figure 8b were fitted with the expression of Eq. (8) (see also Eq. (3)). The corresponding parameters for the large and small domains of the membrane are compiled in Table 1. The parameters $\bar{\varphi}_{min}$ and A are determined as $\bar{\varphi}_{min} = \left(\bar{\rho}_{Mem} - \rho_{H_2O}\right) / \left(\rho_{D_2O} - \rho_{H_2O}\right)$ and $A = 2\pi^2 (\rho_{D_2O} - \rho_{H_2O})^2 \times \Phi_P \left(1 - \Phi_P\right)$, respectively in case of a two-phase system with the volume fractions Φ_P and $\Phi_C = (1 - \Phi_P)$ of the membrane polymers and cavities, respectively. We may interpret the parameter $Q2_{const}$ as the secondary moment from closed cavities and/or precipitates and which is within error bar the same.

Table 1. Parameters from the fit of the second moment Q2 in Figure 8b.

Conditions	Domains	$\bar{\varphi}_{min}$	A [10^{-3} cm^{-1} Å^{-3}]	$Q2_{const}$ [10^{-4} cm^{-1} Å^{-3}]	$\bar{\rho}_{Mem}$ [10^{10} cm^{-2}]
Background scattering in salt-free water	Small	0.36±0.01	9.56±0.46	3.9±0.4	1.93±0.06
	Large	0.23±0.03	10.7±2	3.1±1.2	1.03±0.21

The scattering centers of 0.21 μm average R_g (Table A2) show a minimum at 36% D_2O content (i.e. $\bar{\rho}_{Mem} = \left(1.93 \pm 0.06\right) \times 10^{10}\,\mathrm{cm}^{-2}$) which is in correspondence with the scattering length density of polyester and polysulfone (Table A1). On basis of the above discussion we identified the smaller "domains" as cavities located in the non-woven polyester support layer. The larger

scattering centers of 0.77 μm average R_g (Table A2) show their matching condition at the smaller D_2O content of 23%. The different values for matching of the larger and smaller scattering centers are strong indication that they belong to different layers of the membrane, i.e. the larger ones should be part of the polyamide - polysulfone composite layers. The scattering length density of $\rho = 1.03\times10^{10}$ cm^{-2} (Table 1) of the larger scattering centers may be represented by polyamide domains ($\rho = 3.14\times10^{10}$ cm^{-2}) protruding into the polysulfone ($\rho = 2.08\times10^{10}$ cm^{-2}) layer (thereby forming precipitates) whose scattering is determined by the square of $\Delta\rho = 1.06\times10^{10}$ cm^{-2} as determined from the difference of ρ from both components.

After identification of the scattering cross-sections and determining the SANS parameters as compiled in Tables 1 and A2 we evaluated the structural parameters of the membrane as summarized in Table 2. For this analysis we have chosen the SANS data obtained for the membrane measured in air with no water involved. The second and 3rd columns from the left show the coherent scattering length density as determined in Table 2 as well as the radius of gyration R_g directly determined from the fit of Eq. (1) and (2). The domain volume V_P was determined from the ratio of $d\Sigma/d\Omega(0)$ and Q2 of Eqs. (2), (3), which eliminates volume fraction as well as scattering contrast. For spherical shape domains the determined radius R is consistent

Table 2. Parameters derived from the SANS parameters in Table A2 for the measurement in air for a non-woven polyester fabric

Sample	ρ [10^{10} cm^{-2}]	R_g [μm]	V_P [10^{-14} cm^3]	$\Phi_P\times(1-\Phi_P)$	N_P [10^{12} cm^{-3}]	$N_P \times S_P$ [10^4 cm^{-1}]
Polyester non-woven fabric	2.02	0.26±0.02	4.6±0.9 (R=0.22±0.02 μm)	0.28×0.72	6.2±1.2	4.97±0.27 (R=0.25 μm)
Polyamide/ polysulfone	1.03	0.83±0.01	323±17 (R=0.92±0.02 μm)	0.4×0.6	(7.4±0.4)×10^{-2}	0.78±0.18 (R=0.92 μm)

with R_g. The 5th row presents the domain volume fraction as derived from Q2 in Eqs. (3) and (8) and $\Delta\rho^2 = \rho^2$ in the first column. As the non-woven fabric is about 100 μm thick out of total

membrane thickness of 140 μm we had to multiply the product $\Phi_P\left(1\text{-}\Phi_P\right)$ with 1.4 in order to adjust the sample thickness of $d\Sigma/d\Omega(0)$ to the non-woven part only. Identifying Φ_P = 0.28 as volume fraction of polyester we determined a domain number density $N_P = \Phi_P / V_P$ according to the values in column six. The total surface per unit volume cm^3 is shown in the last column. The Porod constant P_4 in Eq. (2) divided by the scattering contrast is delivering this number. Considering N_P and assuming again spherical shape domains one gets again consistent values with respect to the radius R.

The polyamide/ polysulfone scattering domains are consistently determined with respect to their size and number density. However, the volume fraction of these domains is of the order of 50% even though distributed over total membrane volume. This is from our comprehension a strange result as these domains should only form in the neighborhood of the much smaller polyamide/ polysulfone interface. SANS studies of polyamide - polysulfone composite layers and in particular its polyamide skin part were previously reported by Singh et al. [35]. The authors measured in a Q range between 0.018-0.35 $Å^{-1}$ being sensitive to domain sizes from about 20 to 300 Å. They found that the polyamide skin layer was built up of about 240 Å large compact blocks. A comparison of the RO polysulfone – polyamide composite and of the neat polysulfone gave weak scattering from the polyamide skin layer showing strong correlation between domains of about 140 Å size and volume fraction of 0.7 in consistence with the block units found in aqueous solution. The scattering was dominated by the polysulfone layer because of its much larger thickness.

Such strong scattering cannot be caused by clean (i.e. homogeneous phase) and compact micro-porous material. Appreciable volume fraction of chemical heterogeneities (that may be also referred to as precipitates) must exist within and at the interface of the micro-porous membrane layer in order to explain the scattering of neutrons observed by the authors of ref [35,36] as well as the determined scattering length density of the larger domains in the present study (Figure 8). Such heterogeneities were indeed observed from SEM and TEM by Freger [37].

4.2. **SANS membrane characterization in the RO-Cell**

In this section real-time SANS experiments on a TFC RO membrane mounted in the RO pressure cell are presented. The feed is a simulated secondary effluent (SSE) as outlined in our previous studies [8,9,10]. The scattering length density ρ of the SSE solution was adjusted by using 40% of D_2O mixture of water in order to minimize scattering from cavities in particular from the smaller ones of the membrane (Figure 8b). In parallel to the SANS experiments the permeate flux through the membrane was determined.

4.2.1. Neutron total Scattering Cross-section and Permeate Flux

Figure 9 shows the linear coefficient (μ_t = - ln(T)) derived from the SANS transmission coefficient T (Eq. (5)), the accumulated volume of the permeate and the permeate flux of a TFC

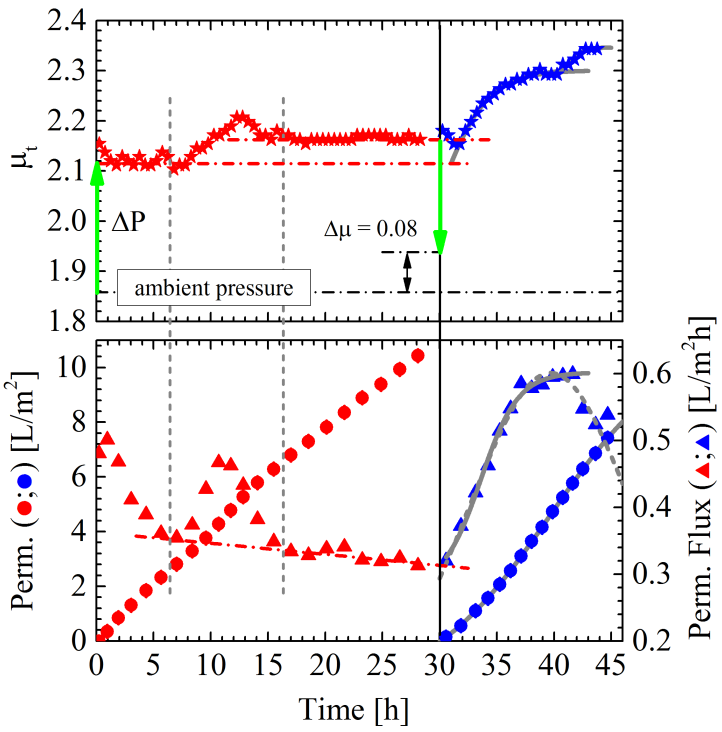

Figure 9. Total scattering cross-section Σ_t derived from neutron transmission (★;★) (top) and permeate accumulated volume(●;●) and permeate flux (▲;▲) (bottom) as a function of time. Water composition was 40% D_2O and 60% H_2O and transmembrane pressure ΔP = 6 bar.

RO-membrane at 6 bar over a period of 45 hours. During the first 30 hours the SSE solution was used as feed which was then replaced by a fresh SSE solution that contained 5 mg/L of BSA. Before starting the experiment the membrane was equilibrated in the cell with SSE for 12 hours at ambient pressure. During the first 6 hours of the experiment the permeate flux shows a continuous decline of nearly 33%, that is from 0.52 to 0.35 L/m^{2}h and between 7 and 16 h a hump with a maximum of 0.46 L/m^{2}h before it stabilizes at about 0.33 L/m^{2}h. The 33% decline of permeability during the first 6 hours may be caused by accumulation of some colloids from the SSE at the membrane surface or from compaction of the membrane (which is less likely due to the rather low applied pressure). The linear coefficient (μ_t) declines during the first 2 hours before showing two distinct time intervals of fairly constant values, namely of 2.12±0.01 and 2.166±0.006 below 7.5 h and above 16.5 h, i.e. above 16.5 h an enhancement of $\Delta\mu = (4.6\pm0.03)\times10^{-2}$ is found which corresponds to a stronger scattering of $\Delta\Sigma = 3.29\pm0.02$ cm^{-1} considering the membrane as the origin of enhanced scattering (D_S = 140 μm). The correspondence of the peaks of μ_t and permeate flux between 11-13 hours should be noted.

We also measured μ_t in absence of trans-membrane pressure (cross-flow valve was fully open) before applying 6 bar and after 30 hours as indicated by the horizontal dashed dotted lines in Figure 9 (top). Both values of μ_t show an enhancement of $\Delta\mu = 0.08$ or $\Delta\Sigma = 5.71$ cm^{-1} larger than $\Delta\mu$ above 16.5 h at 6 bar. The increment of $\Delta\Sigma$ indicates changes of the membrane itself caused by irreversible scaling and/or internal fouling during the 30 hours exposure of the SSE feed. The corresponding differential scattering cross-section $d\Sigma/d\Omega(Q)$ is shown below in Figure 10b.

A further observation is the nearly reversible enhancement and decline of μ_t by about 14 and 12%, respectively, when applying and relaxing 6 bar as indicated by the two green arrows in Figure 9. We interpret the pressure induced enhancement of scattering by compression of the polyester non-woven layer whose structural parameters are collected in Table 2. The product of the volume fractions of polymer and cavity $\Phi_P(1-\Phi_P)$ determined as 0.28×0.72=0.2 is proportional to scattering intensity (Eqs. (2) and (3)). The increase of μ_t could be explained by a 14% enhanced value of the product of the volume fractions according to 0.35×0.65=0.228. It is reasonable that this value corresponds to a decrease of cavity volume alone as the volume of

polyester should not be affected by pressure. The reduction of volume leads to a reduction of the polyester layer thickness from 100 μm to ~ 80 μm. Other effects such as the small increase of SSE volume (ca 1.4%) and compressibility of the feed (0.1%) are negligible.

The blue symbols in Figure 9 show the resulting effects of the BSA containing SSE solution. Surprisingly, the addition of BSA continuously enhances the permeate flux for about 10 hours to a maximum value of 0.60 L/m^2 h, i.e. doubling the permeate flux before it is starting to decline again as well as the corresponding μ_t to an overall enhancement from 2.166±0.005 to 2.3±0.001. Both, the permeate flux and the corresponding μ_t could be specified by the Boltzmann equation (Appendix B, Eq. (B1)) as shown from the two fits in Figure 9, depicted as solid grey lines, delivering a time constant of τ = 1.6±0.3 h and τ = 2.1±0.4, respectively. Above 10 hours after the addition of BSA the permeate flux declines whereas the scattering further increases to a μ_t = 2.35±0.003. Within experimental error the time constants for permeate flux and neutron scattering intensity expressed by $\Delta\mu$ are the same and are an indication of correlated behavior. It should be noted that scattering of the scaling layer is dominated by the calcium minerals as BSA has a very low scattering contrast because of the 40% volume fraction of D_2O of the SSE feed (Figure 1).

A similar effect of membrane cleaning was observed by R. Higgin et al. [38] for the behavior of silica fouling in the presence of alginate. In their case, a 20% flux reduction was almost totally recovered by the addition of alginate.

4.2.2. SANS Scattering Data

Figures 10 and 11 show Q dependent scattering data accumulated in the course of desalination of the SSE feed in the SANS RO-cell, and correspond to the linear coefficient μ_t or neutron cross-section Σ_t and permeate flux data of Figure 9 at distinctive times. Whereas the total scattering cross-section Σ_{SANS} (Eq. (6)) as part of Σ_t represents the integral of the total scattered neutrons the differential scattering cross-section $d\Sigma/d\Omega(Q)$ such as those depicted in Figure 10 is determined as a function of Q over the finite Q interval of 2×10^{-4} and 2.5×10^{-3} in units of Å^{-1}. This range of Q is sensitive for scattering from domains of dimensions between 0.1 and 1μm which appeared within the relevant length scale of the membrane micro-structures (section 4.2)

and domains forming membrane scaling [8,10]. The parameter Σ_{SANS} provides important hints about scattering occurring somewhere in Q, whereas the differential cross-section, $d\Sigma/d\Omega(Q)$ allows determination of detailed quantitative parameters of the scattering domains. We have to mention again that scattering from cavities in polysulfone as well as in polyester non-woven fabric and BSA is fairly well matched in SSE with 40% D_2O content.

The data in Figure 10a show scattering curves measured before applying pressure across the membrane (Red dots; SSE feed no BSA added) and after 30 hours, when finishing the desalination process (blue triangles). The corresponding linear coefficients are depicted as horizontal dashed-dotted lines in Figure 9. Both curves represent scattering from the membrane

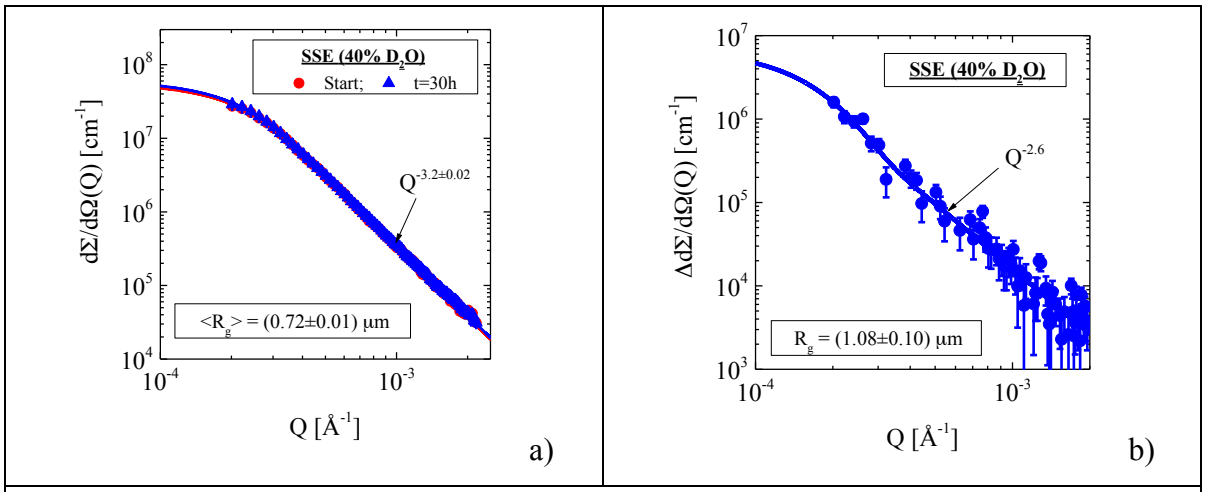

Figure 10. SANS results in the absence of applied pressure. a) Scattering before and after 30 h of exposure of SSE at 6 bar. The transmission coefficients of both curves are depicted as red arrows in the left part of Figure 9. b) Difference from both scattering patterns showing enhanced scattering from membrane after 30 hours of SSE exposure.

only and a possible scaling layer formed during 30 hours of desalination. The scattering of the membrane at both conditions is similar in shape with respect to the scattering from the membrane measured in 40% D_2O salt free water (Figure 8a). Subtraction of both curves shows that the desalination treatment indeed led to an enhanced scattering by about 5% at $Q = 2\times10^{-4}$ $Å^{-1}$, i.e. it induced a positive $\Delta d\Sigma/d\Omega$ as depicted in Figure 10b. The parameters of this analysis are compiled in Table 3. The first moment (Eq. (7)) of $\Delta d\Sigma/d\Omega$ was evaluated as 0.145 $cm^{-1}Å^{-2}$ from which the cross-section $\Delta\Sigma_{SANS}$ = 3.78 cm^{-1} and $\Delta\mu$ = 0.053 (D_S = 140 μm) was derived. The corresponding linear coefficients derived from transmission (dashed dotted lines in Figure 9)

deliver a slightly larger $\Delta\Sigma_{SANS}$ = 5.64 cm^{-1} ($\Delta\mu$ = 0.08) indicating additional scattering from smaller particles outside the range of Q in Figure 10. The radius of gyration of the formed

Table 3: Parameters of RO-membrane obtained from SANS data in Figure 10.

Time [h]	$d\Sigma/d\Omega(0)$ [10^7 cm^{-1}]	R_g [μm]	P_α [10^{-5} cm^{-1} $Å^{-\alpha}$]; (α)	Σ_{SANS} [cm^{-1}] +)	$\Delta\mu$
0	5.67±0.12	0.71±0.07	9±0.8 (3.2±0.02)	--------	--------
30 h	6.16±0.10	0.73±0.06	10.2±0.8 (3.2±0.01)	---------	--------
$\Delta d\Sigma/d\Omega$ after 30 h	0.69±0.18	1.08±0.1	(2.54±0.17)×10^{-4} (2.6)	3.78	0.053

scattering domains is of the order of 1 μm and these domains show scattering following a power law of α = 2.6 at large Q. The exponent α of such power laws is characteristic for the shape of domains as it determines their fractal dimension such as the exponent α = 2.6 characterizing an open mass fractal structure [23].

The increment of $\Delta d\Sigma/d\Omega(Q)$ when no pressure is applied to the membrane has its origin from scaling and/or internal fouling of the membrane alone as no concentration polarization and reversible compression of the membrane takes place. The situation is different for the other two $\Delta d\Sigma/d\Omega(Q)$ in Figure 11a and b measured during the process of desalination at 6 bar and subtracted with the same $d\Sigma/d\Omega(Q)$ measured at ambient pressure. Figures 11a and b show $\Delta d\Sigma/d\Omega(Q)$ after 2 and 13 hours of treatment the SSE feed and at 1 and 9 hours after adding 5 mg/L BSA to the SSE, respectively. The increase of scattering at 2 hour is mainly caused from membrane compaction as discussed in the former section whereas the further increase of $\Delta d\Sigma/d\Omega(Q)$ at 13 hours results from membrane scaling. This result supports the interpretation of the data in Figure 9 showing a maximum in permeate flux and total cross-section.

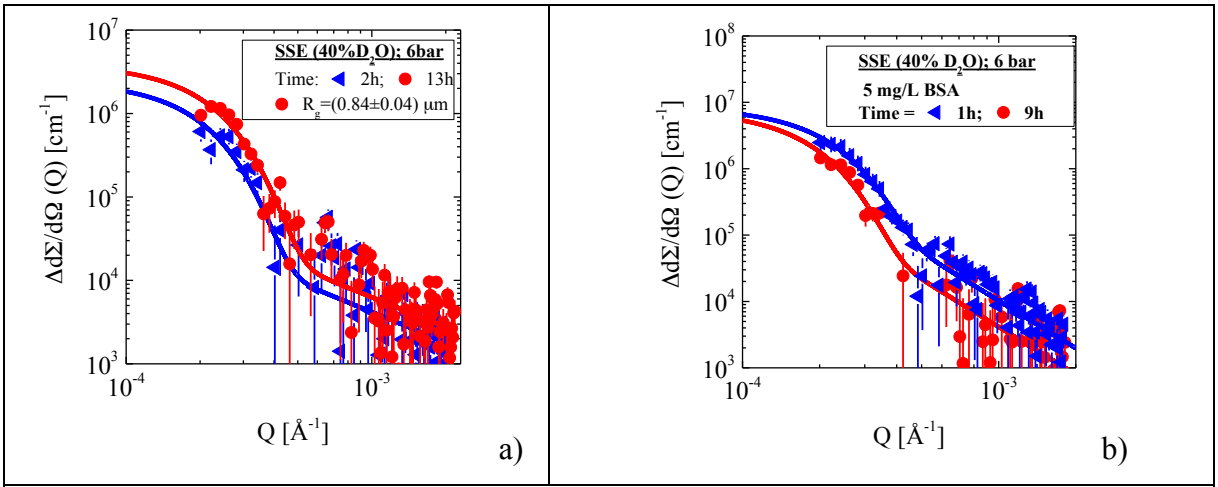

Figure 11. SANS results obtained during RO experiment from membrane exposed to SSE feed at 6 bar. a) Membrane after treatment for 2 and 13 hours. The increase of scattering in corresponds to the minimum of transmission on the left side of Figure 9. b) $\Delta d\Sigma/d\Omega(Q)$ at 2 and 9 hours after addition of 5 mg/L BSA to the SSE feed.

On the other hand 9 hours after adding BSA to the SSE solution an overall decline of scattering by roughly a factor of 2 is observed in the measured Q range (Figure 11b), corresponding to the maximum of permeate flux in Figure 9b. The decline of $\Delta d\Sigma/d\Omega(Q)$ gives the information that μm large scattering centers diminished and disappeared from the volume of the feed exposed to neutron irradiation. This observation appears consistent with the observed increasing permeate flux in Figure 9. On the other hand the linear coefficient in Figure 9 (right side) shows an increment of $\Delta\mu = 0.13$. This means that enhanced scattering must occur at some Q larger than 2×10^{-3} $Å^{-1}$ outside the Q range of our experiment, i.e. these particles must be smaller in size. It is known from former work [8], that in a first stage BSA induces mineralization of organic-inorganic composites of about R_g = 0.5 μm. Nevertheless, these phenomena demonstrate again the strong relationship between the membrane permeability and fouling behavior and its response to transmission/scattering of neutrons.

In searching for an explanation of the data from the last two sections it has to be admitted that the origin of the permeate flux hump at 7-16 h in Figure 9 (left side) is not yet clear. It may be caused by partially detaching of rather large scale mineral particles from the membrane surface due to drag forces exerted by the flowing solution. It is more likely to have this happen at the low pressure level used in this study as the adherence of any fouling layer (scale, biofilm etc.)

to the membrane surface cannot be that strong as well as the layer itself may be less compact compared to those obtained at the standard operative pressures of these membranes. This action may partially clean the membrane, resulting in a temporal increase of permeate flux. This explanation is supported by the associated maximum of μ_t at 12 h due to enhanced scattering by these large scale domains in Figure 11a. This rationalization is also supported by the behavior in the presence of BSA as described on the right side of Figure 9. The enhancement of flux after the addition of BSA is also associated with a significant enhancement of μ_t (from 30 to 40 h). Likewise, the enhanced flux may be caused by rather large scale domains detached from the membrane surface. However, the diffraction data in Figure 11b show a decline by a factor of 2 from scattering of μm large particles. This observation is consistent with the picture of correlated enhanced flux and detachment of large particles from the membrane surface; however, it is in contrast to enhanced μ_t indicating that scattering domains of smaller size must exist at larger Q outside the experimental range.

5. Summary and Outlook

The goal of the present study was to demonstrate the use of SANS in following *in-situ* scaling and fouling of TFC membranes during RO wastewater desalination close to realistic conditions. A special RO-cell was designed to enable collecting SANS spectra and permeate flux data simultaneously at pressures up to 6 bar. The results show a complex situation because the neutrons have to pass through several sections of the cell such as feed, the three layers of the TFC membrane, the spacer, as well as a possible layer formed by fouling and scaling at the membrane surface. The signal from the membrane may deliver valuable information on the internal membrane structure and fouling if the scattering contrast of the membrane is properly adjusted by the D_2O content of the feed (Figure 8), or by separating scattering from the individual layers of the membrane [35].

The outcome of this study can be summarized in three sections:

(i) In a first step scattering from a TFC membrane exposed to air and salt-free water was analyzed by contrast variation SANS technique (Figures 6-8). Scattering from two types of domains were identified, namely cavities (R_g= 0.2 μm) of the nonwoven polyester

support layer (Figure 8b and Table A1) and polyamide precipitates (R_g= 0.9 μm) in the polysulfone layer. However, the volume fraction of the polyamide precipitates came out far too large occurring only in the limited part of the polysulfone layer. At large Q (Figure 6) weak scattering from rod-like cavities of ~300 Å diameters were identified being a relevant part of the micro-porous polysulfone layer [34].

(ii) Permeate flux, SANS scattering cross-section (Σ_{SANS}) derived from neutron transmission, as well as diffraction data ($d\Sigma/d\Omega(Q)$) are the outcome of our real-time desalination experiments (Figures 9 to 11). The linear coefficient $\mu_{SANS} = \Sigma_{SANS} \times D_S$ shows an overall enhancement accompanied by a reduced membrane permeability (Figure 9). The appreciable enhancement of membrane permeability after the addition of BSA to the feed might be emphasized. The corresponding diffraction data in Figure 11b show a decline of scattering by a factor of 2 as interpreted from detachment of large particles from the membrane surface. On the other hand the enhancement of μ_t is a strong indication of enhanced scattering from smaller particles at larger Q outside of our Q window.

(iii) Upon completion of the desalination process after 30 h, SANS was measured in the absence of applied pressure and compared with data just taken before starting desalination. In this way we eliminated effects from concentration polarization and membrane compressibility and were only sensitive to changes of the membrane alone. The enhancement of scattering, $\Delta d\Sigma/d\Omega(Q)$, is depicted in Figure 10b and shows particles of the order of 1 μm radius of gyration with an open mass fractal structure according to the power law exponent of $\alpha = 2.6$.

In summary, the presented study with the *in-situ* RO-SANS setup is a first demonstration of using SANS for exploring membrane performance and fouling at RO conditions. It became clear from the present experiments that additional measurements have to be performed at larger Q in order to become sensitive to even smaller particles. Furthermore, improvements are necessary such as the ability to distinguish between the scattering signals from feed, fouling layer and membrane. One step in this direction will be to measure the feed separately in a second cell implemented in the cross flow circle.

Acknowledgements

This work was funded partially by the Ministry of Science, Culture and Sport (MOST), Israel and the Bundesministerium für Bildung und Forschung (BMBF), Germany as part of the joint German–Israeli Water Research Program (grant no. WT0902), and by the German-Israeli Foundation for Scientific Research and Development (GIF), grant no. I-101-307.4-2013. The neutron experiments were performed at the KWS 2 and 3 instruments operated by JCNS at the Heinz Maier-Leibnitz Zentrum (MLZ), Garching, Germany. D.S. would like to particularly thank Prof. Dieter Richter, head of the institute Neutron Scattering at "Institute of Complex Systems" and "Jülich Centre for Neutron Science" at Forschungszentrum Jülich, and Prof. Winfried Petry, scientific director of the research neutron source Heinz Maier-Leibnitz (FRM-II) in Garching, for their hospitality and support of the present project.

7. Appendices

A. Relevant SANS Parameters

In this section we present relevant parameters for SANS such as the coherent scattering length density of water, molecules of the TFC membranes, and minerals.

Table A1
SANS relevant parameters of membrane polymers and minerals which could be formed at the surface of the membrane during desalination

Molecule	Chemical formula	Mass density [g/cm^3]	Molar weight [g/mol]	ρ [10^{10} cm^{-2}]	Φ_{match}
Water	H_2O/D_2O	1/1.107	18.02/20.03	$\rho_{Water} = -0.560 + 6.933 \times \Phi_{D_2O}$	---
Polysulfone	$C_{27}H_{22}O_4S$	1.24	442.54	2.08	0.38
Aromatic Polyamide	$N_2C_{14}H_{12}O_2$	1.44	238	3.14	0.53
Polypropylene	C_3H_6	0.91	42.08	- 0.325	0.034
Polyester	$C_{17}H_{18}O_4$	1.103	268	1.75 [39] (2.02 [40])	0.33 (0.37)
Calcium phosphate (HAP)	$Ca_5(PO_4)_3(OH)$	3.16	502.31	$4.19+0.391 \times \Phi_{D_2O}$	0.73
Calcite	$CaCO_3$	2.72	100.09	4.76	0.77

Table A2
SANS parameters of reference XLE-440 TFC RO-membrane as measured in the present study.

Sample	$d\Sigma/d\Omega(0)$ [10^6 cm^{-1}]	R_g [μm]	P_4 [10^{-6} cm^{-1} $Å^{-4}$]	Q2 [10^{-3} cm^{-1} $Å^{-3}$]	R^* [μm]	R^{**} [μm]
Small Scattering Centers						
H_2O	2.63±0.25	0.22±0.01	1.58±0.05	1.66	0.195	0.11
Air	2.64±0.48	0.26±0.02	0.91±0.05	1.14	0.222	0.13
10% D_2O	1.62±0.18	0.23±0.01	0.92±0.03	0.98	0.198	0.112
20% D_2O	0.99±0.12	0.23±0.01	0.59±0.02	0.62	0.196	0.11
30% D_2O	0.35±0.05	0.19±0.01	0.42±0.03	0.39	0.162	0.097
40% D_2O	0.55±0.02	0.19±0.04	0.52±0.03	0.50	0.173	0.10
50% D_2O	0.53±0.06	0.19±0.01	0.48±0.01	0.46	0.176	0.10
70% D_2O	3.24±0.24	0.26±0.01	1.28±0.03	1.51	0.216	0.124
100% D_2O	Strong multiple scattering					
Large Scattering Centers						
H_2O	105±2	0.82±0.01	0.197±0.01	0.755	0.87	0.40
Air	83.0±1.6	0.83±0.01	0.052±0.012	0.507	0.938	1.02
10% D_2O	89.1±2.2	0.87±0.01	0.078±0.006	0.53	0.925	0.712
20% D_2O	69.3±2.5	0.91±0.01	0.078±0.003	0.447	0.90	0.60
30% D_2O	53.2±1.4	0.84±0.01	0.107±0.002	0.503	0.793	0.492
40% D_2O	64.9±1	0.91±0.01	0.24±0.04	0.90	0.698	0.393
50% D_2O	42.0±0.66	0.73±0.01	0.150±0.004	0.60	0.691	0.419
70% D_2O	74.5±0.67	0.56±0.01	1.04±0.033	2.83	0.499	0.285
100% D_2O	Strong multiple scattering					

*) Radius R determined from the ratio of $d\Sigma/d\Omega(0)$ and Q2, delivering according to Eq.(2) and (3) the domain volume. R was evaluated on basis spherical shape domains.

B. Analysis of Linear Coefficient from Neutron Transmission and Permeate Flux of RO-Membrane exposed to BSA-SSE

Permeate flux and linear coefficient (determined from neutron transmission) are depicted in Figure 9 after 30 hours exposition of SSE at 6 bar. The enhancement of both parameters could be fitted with the Boltzmann equation

$$P(t)=\frac{P_1-P_2}{1+\exp\left[\left(t-t_0\right)/\tau\right]}+P_2 \qquad \text{(B1)}$$

whose parameters and results are compiled in Table B1 and depicted as solid gray lines in Figure 9, respectively. The time constant τ of neutron and permeate flux measurements are within error bars the same indicating that permeate flux and SANS are measuring the same process.

Table B1

Parameters of Eq. (B1) describing membrane permeate flux and neutron linear coefficient

	τ [h]	P_1	P_2	t_0 [h]
Permeate Flux [L/m^{2}h]	1.63±0.21	0.283±0.023	0.602±0.006	33.6±0.3
Neutron Linear Coefficient	2.14±0.41	1.77±0.43	2.3±0.004	29.7±2.7

References

[1] E.M. Vrijenhoek, S. Hong, et al., Influence of membrane surface properties on initial rate of colloidal fouling of reverse osmosis and nanofiltration membranes, J. Membr. Sci. 188(1) (2001) 115-128.

[2] S. Lee, M. Elimelech, Relating organic fouling of reverse osmosis membranes to intermolecular adhesion forces, Environmental Science & Technology 40(3) (2006) 980-987.

[3] M. Herzberg, M. Elimelech, Biofouling of reverse osmosis membranes: Role of biofilm-enhanced osmotic pressure, J. Membr. Sci. 295(1-2) (2006) 11-20.

[4] R.Y. Ning, T. L. Troyer, Colloidal fouling of RO membranes following MF/UF in the reclamation of municipal wastewater, Desalination 208(1-3) (2007) 232-237.

[5] G. Greenberg, D. Hasson, R. Semiat, Limits of RO recovery imposed by calcium phosphate precipitation, Desalination 183 (2005) 273-288.

[6] Z. Steiner, H. Rapaport, Y. Oren, R. Kasher, Effect of surface-exposed chemical groups on calcium-phosphate mineralization in water-treatment systems, Environmental Science & Technology 44 (2010) 7937–7943.

[7] S. Mann, Biomineralization, Oxford University Press, Oxford 2001.

[8] V. Pipich, Y. Dahdal, H. Rapaport, R. Kasher, Y. Oren, D. Schwahn, Effects of biological molecules on calcium mineral formation associated with wastewater desalination as assessed using small-angle neutron scattering. Langmuir 29 (2013) 7607-7617.

[9] Y.N. Dahdal, V. Pipich, H. Rapaport, Y. Oren, R. Kasher, D. Schwahn, Small-angle neutron scattering studies of alginate as biomineralizing agent and scale initiator, Polymer 85 (2016) 77-88.

[10] Y.N. Dahdal, V. Pipich, H. Rapaport, Y. Oren, R. Kasher, D. Schwahn, Small-angle neutron scattering studies of mineralization on BSA coated citrate capped gold

nanoparticles used as a model surface for membrane scaling in RO wastewater desalination, Langmuir 30 (2014) 15072-15082.

[11] D. Schwahn, D. Richter, M. Lin, L.J. Fetters, The co-crystallisation of a poly(ethylene-butene) random copolymer with C_{24} in n-decane, Macromolecules 35 (2002) 3762- 3768.

[12] D. Richter, M. Monkenbusch, D. Schwahn, Structure characterization in Fourier space - Neutron scattering in polymer science: A comprehensive reference, 2 (2012) 331-361, Elsevier, July 2012.

[13] T.J. Su, J.R. Lu, Z.F. Cui, B.J. Bellhouse, R.K. Thomas, R.K. Heenan, Identification of the location of protein fouling on ceramic membranes under dynamic filtration conditions, J. Membr. Sci. 163 (1999) 265-275.

[14] F. Pignon, A. Magnin, J.-M. Piau, B. Cabane, P. Aimar, M. Meireles, P. Lindner, Structural characterisation of deposits formed during frontal filtration, J. Membr. Sci., 174 (200) 189-204.

[15] E. Kujundzic, A.R. Greenberg, M. Peterson, Review: Ultrasonic characterization of membranes, Desalination and Water Treatment, 52 (7-9) (2014) 1217-1249.

[16] S.T.V. Sim, S.R. Suwarno, T.H. Chong, W.B. Krantz, A.G. Fane, Monitoring membrane biofouling via ultrasonic time-domain reflectometry enhanced by silica dosing, J. Membr. Sci. 428 (2013) 24-37

[17] G. An, J. Lin, J. Li, X. Li, X. Jian, Non-invasive measurement of membrane scaling and cleaning in spiral-wound reverse osmosis modules by ultrasonic time-domain reflectometry with sound intensity calculation, Desalination 283 (2011), 3-9.

[18] J. Cen, M. Vukas, G. Barton, J. Kavanagh, H.G.L. Coster, Real-time fouling monitoring with electrical impedance spectroscopy, J. Membr. Sci., 484 (2015) 133-139.

[19] L.N. Sim, J. Gu, H.G.L. Coster, A.G. Fane, Quantitative determination of the electrical properties of RO membranes during fouling and cleaning processes using electrical impedance spectroscopy, Desalination 379 (2016) 126-136.

[20] J. Cen, J. Kavanagh, H.G.L. Coster, G. Barton, Fouling of reverse osmosis membranes by cane molasses fermentation wastewater: detection by electrical impedance spectroscopy techniques, Desalination and Water Treatment 51(4-6) (2013) 969-975.

[21] Cen, J.; Vukas, M.; Barton, G.; Kavanagh, J.; Coster, H. G. L., Real time fouling monitoring with electrical impedance spectroscopy, Journal of Membrane Science (2015), 484, 133-139

[22] A. Antony, T. Chilcott, H.G.L. Coster, G. Leslie, In situ structural and functional characterization of reverse osmosis membranes using electrical impedance spectroscopy, Journal of Membrane Science 425-426 (2013) 89-97.

[23] R.J. Roe, Methods of X-ray and neutron scattering in polymer science, University Press, Oxford, 2000, p. 188.

[24] Neutron News 3 (1992) 29−37.

[25] B. Jacrot, The study of biological structures by neutron scattering from solution, Rep. Prog. Phys. 39 (1976) 911-953.

[26] G. Beaucage, Approximations leading to a unified exponential power-law approach to small-angle scattering, Journal of Applied Crystallography 28 (1995) 717-728.

[27] G. Porod, General Theory, in: O. Glatter and O. Kratky (Eds.), Small-angle X-ray scattering, Academic Press, New York, 1982, 17-51.

[28] W. Schmatz, T. Springer, J. Schelten, K. Ibel, Neutron small-angle scattering: experimental techniques and applications, J. Appl. Cryst. 7 (1974) 96-116.

[29] H. Frielinghaus, V. Pipich, A. Radulescu, M. Heiderich, R. Hanslik, K. Dahlhoff, H. Iwase, S. Koizumi, D. Schwahn, Aspherical refractive lenses for small-angle neutron scattering. J. Appl. Cryst. 42 (2009) 681-690.

[30] B. Alefeld, D. Schwahn and T. Springer, New developments of small-angle neutron scattering instruments with focussing, Nucl. Inst. a. Meth. in Physical Research A 274 (1989) 210-216.

[31] J. Palacios, D. Schwahn, H. Rauch, High angular resolution neutron transmission measurements - A proposed nondestructive material testing method, NDT International, August 1981, 189-193.

[32] R. Kasher, Membrane-based water treatment technologies: Recent achievements, and new challenges for a chemist, Bulletin of the Israel Chemical Society 24 (2009) 10-18.

[33] A.K. Ghosh, R.C. Bindal, S. Prabhakar, P.K. Tewari, Composite polyamide reverse osmosis (RO) membranes – recent developments and future directions, BARC Newsletter 321 (2011) 43-51.

[34] P. S. Singh, S.V. Joshi, J.J. Devmurari, A. P. Rao, P.K. Ghosh, Probing the structural variations of thin film composite RO membranes obtained by coating polyamide over polysulfone membranes of different pore dimensions, J. Membr. Sci. 278 (2006) 19-25.

[35] P. S. Singh, V. K. Aswal, Compacted nanoscale blocks to build skin layers of reverse osmosis and nanofiltration membranes: A revelation from small-angle neutron scattering, J. Phys. Chem. C 111 (2007) 16219-16226.

[36] P.S. Singh, A.P. Rao, P. Ray, A. Bhattacharya, K. Singh, N.K. Saha, A.V.R. Reddy, Techniques for characterization of polyamide thin film composite membranes, Desalination 282 (2011) 78–86

[37] V. Freger, Nanoscale heterogeneity of polyamide membranes formed by interfacial polymerization, Langmuir 19 (2003) 4791-4797.

[38] R. Higgin, K.J. Howe, T.M. Mayer, Synergistic behavior between silica and alginate: Novel approach for removing silica scale from RO membranes, Desalination 250 (2010) 76–81.

[39] W. Burchard, A. Khalyavina, P. Lindner, R. Schweins, P. Friedel, M. Wiemann, A. Lederer, SANS Investigation of global and segmental structures of hyperbranched aliphatic-aromatic polyesters, Macromolecules 45 (2012) 3177-3187.

[40] E. de Luca, R.W. Richards, I. Grillo, S.M. King, Molecular characterization of a hyperbranched polyester. II. Small-angle Neutron scattering, J. Polym. Sci. Part B: Polymer Physics 41 (2003) 1352-1361.